Filling-enforced Dirac nodal loops in nonmagnetic systems and their evolutions under various perturbations

Dexi Shao* and Chen Fang†

Beijing National Laboratory for Condensed Matter Physics, and Institute of Physics, Chinese Academy of Sciences, Beijing 100190, China

(Received 27 January 2020; accepted 21 September 2020; published 19 October 2020)

Based on symmetry analysis, we propose that filling-enforced Dirac nodal loops (FEDLs) in nonmagnetic systems exist and only exist in five space groups (SGs), namely, SG.57, SG.60, SG.61, SG.62, and SG.205. We explore all possible configurations of the FEDLs in these SGs and classify them accordingly. Furthermore, we study the evolutions of the FEDLs under various types of symmetry-breaking perturbations, such as an applied strain or an external field. The results show that FEDL materials can serve as parent materials of both topological semimetals hosting nodal points/loops and topological insulators/topological crystalline insulators. By means of first-principles calculations, almost all materials possessing FEDLs are predicted.

DOI: 10.1103/PhysRevB.102.165135

I. INTRODUCTION

Topological materials have attracted great interest both theoretically and experimentally [1–3] since the proposal of topological insulators (TIs) [4]. Generally, topological materials can be classified into gapped and gapless systems according to the electronic states near the Fermi level. The most famous examples among them are TIs and Weyl semimetals (WSMs) [5–27], respectively. In terms of the gapped systems, the nontrivial topology of the bands can be characterized by a topological invariant which depends on the Bloch wave functions of all the occupied bands in the whole Brillouin zone (BZ). It is well known that symmetries always play key roles in the classification of them. One of the celebrated examples is the "periodic table" of noninteracting TIs and topological superconductors (TSCs) characterized by time-reversal symmetry (TRS), particle-hole symmetry, and chiral symmetry [28,29]. In addition, the crystal symmetries are found to give rise to a new kind of TIs, i.e., the topological crystalline insulators (TCIs) [28,30–34]. Recently, TCIs in nonmagnetic systems have been enumerated [35–37], and these states can be fast diagnosed by symmetry eigenvalues [38–46]. Besides TIs and TCIs, many gapless topological phases have also been proposed, such as Dirac semimetals [47–61], node-line semimetals [62–69], nodal surface semimetals [70–74], hopf-link semimetals [75,76], and many other semimetals with unconventional quasiparticles beyond Dirac and Weyl fermions [77–79]. All these findings have greatly improved our knowledge of both the gapped and the gapless topological phases.

Guided by the compatibility relations [38], many nonsymmorphic-symmetry-enforced degeneracies have been proposed. Especially, there exists a new type of degeneracies which are filling enforced. Fillings that realize a band insulator for all nonsymmorphic space groups (SGs) with and without SOC are listed [80]. Systems with other fillings must be gapless, namely, the filling-enforced semimetals. Until now, many filling-enforced semimetals have been proposed [38,41–43], among which filling-enforced Dirac nodal loop (FEDL) semimetal is a special example with fourfold degenerate nodal loops in the BZ. Different from WSMs which only require lattice translation symmetry for their protection, materials with FEDL require some more symmetries. Although the FEDLs have been proposed in several systems [81–86], a general idea for searching the FEDL materials is still missing.

In this work, we first explore the necessary and sufficient conditions for FEDLs in nonmagnetic systems and find that there are five and only five SGs possessing the FEDLs. Then, we further explore all possible configurations of the Dirac nodal loops and classify them accordingly. Motivated by earlier works [87–90], we study the evolutions of the FEDLs under various perturbations and find that the FEDL materials can serve as parent materials of both various topological semimetals and TIs/TCIs. At last, almost all the FEDL materials are listed, from which we have picked out some good candidates with fewer and smaller electron/hole pockets near the Fermi level by means of first-principles calculations.

II. METHODS

We perform first-principles calculations based on the density functional theory (DFT) using projector augmented wave (PAW) method implemented in the Vienna *ab initio* simulation package (VASP) [91]. The generalized gradient approximation (GGA), as implemented in the Perdew-Burke-Ernzerhof (PBE) functional [92], is adopted to get the band structures. The cutoff parameter for the wave functions was 500 eV. The BZ was sampled by Monkhorst-Pack method [93] with a k spacing of $0.025 \times 2\pi\,\text{Å}^{-1}$ for the three-dimensional periodic boundary conditions.

*sdx@iphy.ac.cn
†cfang@iphy.ac.cn

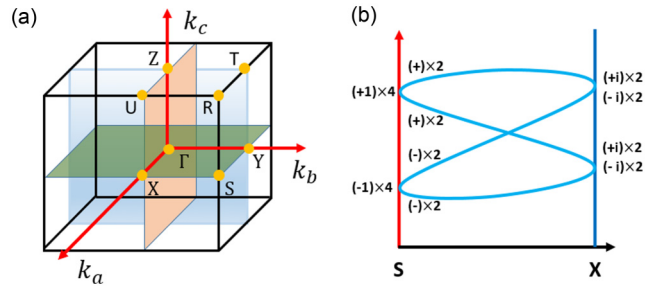

FIG. 1. The schematic figures of (a) the corresponding BZ of SG.61. (b) The hourglass dispersion along S-X. Labels of the vertical axis in the right figure denote G_x eigenvalue g_x. We can find the fourfold degenerate band crossings due to the hourglass dispersion protected by the G_x symmetry between two quartets.

III. RESULTS AND DISCUSSIONS

A. General descriptions of FEDLs

Up to now, there are some FEDL materials proposed in earlier works [83–86]. Among them, AgF_2 in SG.61 is a good example with the hourglass dispersion between S and X in the band structures, as shown in Fig. 1. It is the hourglass dispersion protected by the glide-mirror symmetry G_x that contributes to the FEDL. Different from the hourglass dispersion in the nodal-chain metals [94], the hourglass dispersion leading to the FEDL owns some unique features. The first feature is the existence of the TRS (T) and the inversion symmetry (P), which are required for the locally double degeneracy at each $\vec{k}$ point in the BZ. Secondly, the Dirac nodal loop is always protected by some glide-mirror symmetry G_α and located on the $k_\alpha = \pi$ plane. Here, $\alpha = lx + my + nz$ denotes the normal direction of the glide-mirror symmetry G_α with the Miller indices $\langle lmn \rangle$.

Here we give a general description of a Dirac nodal loop. A Dirac nodal loop is a type of fourfold degenerate nodal loop locating in a time-reversal invariant plane and is constructed by the band crossings of two PT related doublets with opposite mirror/glide-mirror eigenvalues. These band crossings along any path connecting two time-reversal invariant momenta (TRIMs) originate from the hourglasslike dispersion protected by the mirror/glide-mirror symmetry. We say one plane in the BZ is time-reversal invariant if the set of $\vec{k}$ points in this plane map to the same plane up to a reciprocal lattice vector under TRS.

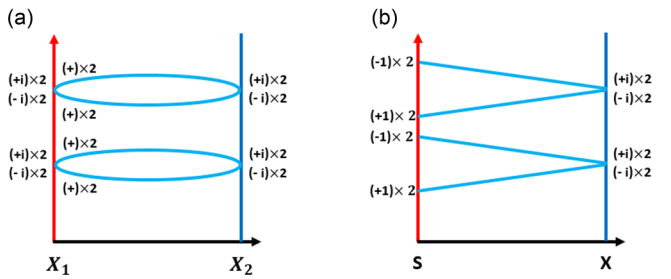

FIG. 2. The schematic figures of band connections between (a) two "X"-type TRIMs and (b) one "S"-type TRIM and one "X"-type TRIM.

TABLE I. The generators of the SGs possessing FEDLs.

Operators	Seitz form
$\hat{E}$	$\{1\|0\}$
$\hat{G}_\alpha$	$\{m_{100}\|\frac{1}{2}\frac{1}{2}0\}/\{m_{100}\|\frac{1}{2}\frac{1}{2}\frac{1}{2}\}$
$\hat{P}$	$\{-1\|0\}$
$\hat{G}_\beta$	$\{m_{010}\|lmn\}$

1. "A/B" in the "Seitz form" column means the expression of the corresponding operator possesses alternative representations.
2. "l," "m," and "n" in $\{m_{010}|lmn\}$ can be either 0 or $\frac{1}{2}$, because $\hat{G}_\beta^2$ and $\hat{R}_{2\beta}^2$ must be integer lattice translation in the real space.

In the following, we will deduce the necessary and sufficient conditions of a FEDL.

(1) The combination of P and T, i.e., PT, gives the local double degeneracy at each $\vec{k}$ point in the BZ, termed as PT related doublets. We only focus on the nonmagnetic systems, thus, P, T, and the combination of them PT are all required.

(2) The existence of a mirror/glide-mirror symmetry $G_\alpha = \{m_\alpha|\vec{\tau}\}$ serves bands within the PT related doublet sharing the same G_α eigenvalues. Following the work by Fang *et al.* [95], bands within the PT related doublet sharing the same G_α eigenvalues appear only if the component of $\vec{\tau}$ along the α direction (denoted by $\vec{\tau}_\alpha$) is a half modulo an integer lattice translation. It should be noted that each component of $\vec{\tau}$ must be either zero or a half modulo an integer lattice translation because G_α^2 is always an integer lattice translation in the real space. Simultaneously, the Dirac nodal loop can only exist in the $k_\alpha = \pi$ plane, while not the $k_\alpha = 0$ plane. It can be seen from the following. In the G_α invariant plane,

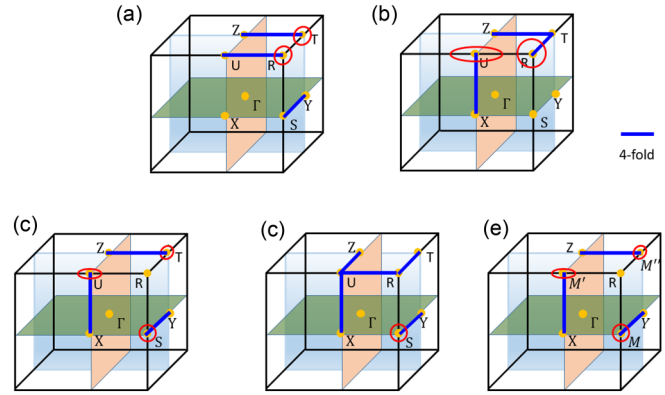

FIG. 3. The schematic figures for the configurations of FEDLs in (a) SG.57, (b) SG.60, (c) SG.61, (d) SG.62, and (e) SG.205, in the BZ, respectively. The nattier blue, pink, and green planes in the figures correspond to the $k_x = 0$, $k_y = 0$, and $k_z = 0$ planes, respectively. The solid blue lines here denote fourfold degenerate states within the $(4n)$th to $(4n + 3)$th bands from the corresponding compatibility relations along these lines. There are two FEDLs encircling R and T in the $k_y = \pi$ plane in SG.57, two FEDLs encircling U/R in the $k_z = \pi/k_x = \pi$ planes in SG.60, three FEDLs encircling S/T/U in the $k_x = \pi/k_y = \pi/k_z = \pi$ planes in SG.61, only one FEDL encircling S in the $k_x = \pi$ plane in SG.62 and three FEDLs encircling M/M′/M″ in the $k_x = \pi/k_y = \pi/k_z = \pi$ planes in SG.205, respectively.

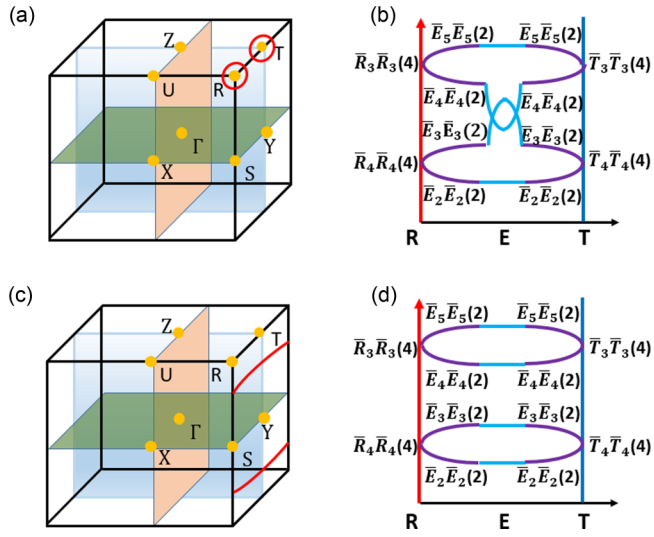

FIG. 4. The schematic figures for the configurations of FEDLs in $k_y = \pi$ plane in SG.57. The two red rings in figure (a) and two red lines traversing the BZ in figure (c) denote the contractible/noncontractible FEDLs in the BZ, respectively. In the corresponding right panels, the purple lines show compatibility relations between high-symmetry momenta $\vec{k}$ (i.e., R and T) and some infinitesimally close momenta $\vec{k} + \delta\vec{k}$ along the R-T line, while the blue lines show band connections between the momentum infinitesimally close to R and the momentum infinitesimally close to T in the R-T line.

we have

$$g_\alpha = \pm ie^{-i\vec{k}_{n\alpha}\cdot\vec{\tau}_{n\alpha}}. \tag{1}$$

Here, g_α denotes eigenvalue of G_α for $\vec{k}$ points in the G_α invariant plane. The component of $\vec{k}$ along the α direction is denoted by $\vec{k}_\alpha$, while $\vec{k}_{n\alpha}$ denotes the other components of $\vec{k}$, i.e., $\vec{k} = \vec{k}_\alpha + \vec{k}_{n\alpha}$. Similarly, $\vec{\tau}_{n\alpha}$ denotes the components of $\vec{\tau}$ along directions other than α, i.e., $\vec{\tau} = \vec{\tau}_\alpha + \vec{\tau}_{n\alpha}$. Furthermore, we denote the magnitudes of $\vec{k}_\alpha$ and $\vec{\tau}_\alpha$ as k_α and τ_α, respectively. Within these notations, we have $k_\alpha = \vec{k}_\alpha \cdot \hat{\alpha}$, $\vec{k}_\alpha = k_\alpha\hat{\alpha}$, $\tau_\alpha = \vec{\tau}_\alpha \cdot \hat{\alpha}$, and $\vec{\tau}_\alpha = \tau_\alpha\hat{\alpha}$. Here $\hat{\alpha}$ denotes the unitary vector along the α direction. Suppose $|\psi\rangle$ is the eigenstate of G_α with $g_\alpha = \pm ie^{-i\vec{k}_{n\alpha}\cdot\vec{\tau}_{n\alpha}}$, then

$$\begin{aligned}
G_\alpha(PT)|\psi\rangle &= (G_\alpha P)T|\psi\rangle \\
&= \left(PG_\alpha T_{2\vec{\tau}_\alpha - 2\vec{\tau}_{n\alpha}}\right)T|\psi\rangle \\
&= PG_\alpha T T_{2\vec{\tau}_\alpha - 2\vec{\tau}_{n\alpha}}|\psi\rangle \\
&= PTG_\alpha T_{2\vec{\tau}_\alpha - 2\vec{\tau}_{n\alpha}}|\psi\rangle \\
&= PTG_\alpha e^{-i2(k_\alpha\tau_\alpha - \vec{k}_{n\alpha}\cdot\vec{\tau}_{n\alpha})}|\psi\rangle \\
&= PTg_\alpha e^{-i2(k_\alpha\tau_\alpha - \vec{k}_{n\alpha}\cdot\vec{\tau}_{n\alpha})}|\psi\rangle \\
&= g_\alpha^* e^{i2(k_\alpha\tau_\alpha - \vec{k}_{n\alpha}\cdot\vec{\tau}_{n\alpha})}PT|\psi\rangle \\
&= \mp ie^{-i\vec{k}_{n\alpha}\cdot\vec{\tau}_{n\alpha}}e^{i2k_\alpha\tau_\alpha}(PT)|\psi\rangle,
\end{aligned} \tag{2}$$

which indicates $PT|\psi\rangle$ is the eigenstate of G_α with $g_\alpha = \mp ie^{-i\vec{k}_{n\alpha}\cdot\vec{\tau}_{n\alpha}}e^{i2k_\alpha\tau_\alpha}$. Thus, requirement of PT related doublets sharing the same G_α eigenvalue means

$$ie^{-i\vec{k}_{n\alpha}\cdot\vec{\tau}_{n\alpha}} = -ie^{-i\vec{k}_{n\alpha}\cdot\vec{\tau}_{n\alpha}}e^{i2k_\alpha\tau_\alpha}, \tag{3}$$

which requires $e^{-i(2k_\alpha\tau_\alpha)} = -1$. Here $T_{2\vec{\tau}_\alpha - 2\vec{\tau}_{n\alpha}}$ denotes the translation operator with translational vector $2\vec{\tau}_\alpha - 2\vec{\tau}_{n\alpha}$. This can be obtained only if $\tau_\alpha = \frac{1}{2}$ modulo an integer lattice translation and $k_\alpha = \pi$.

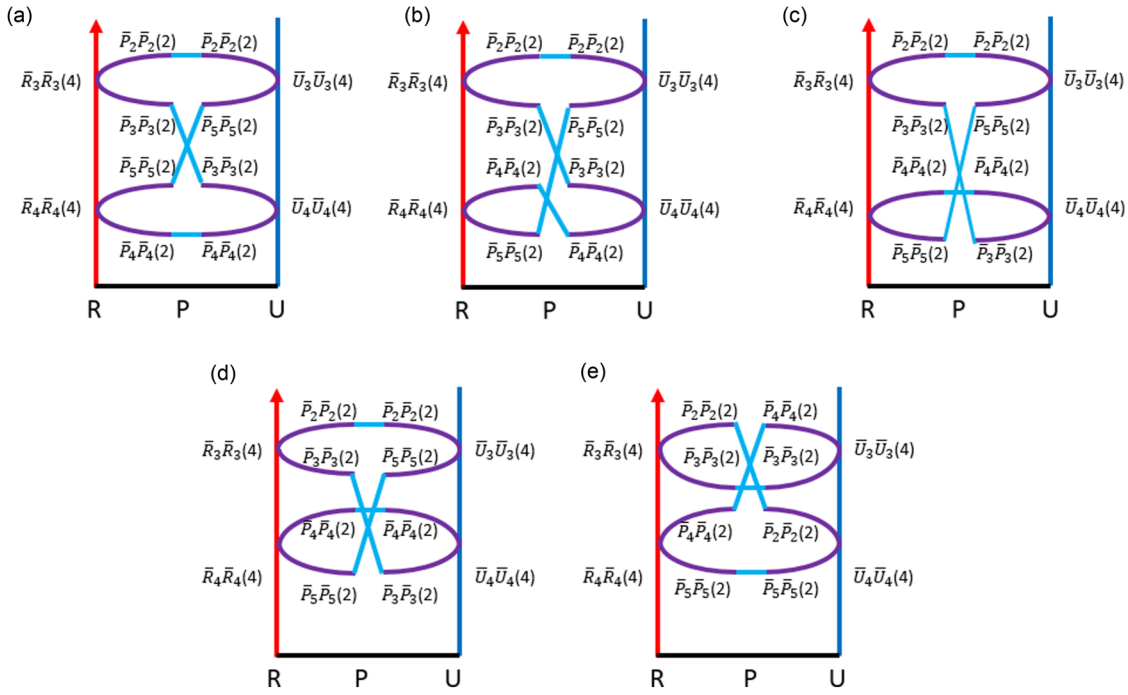

FIG. 5. (a)–(e) Five possible connections of the bands satisfying the compatibility relations along R-U in SG.60.

TABLE II. The operators in SG.61.

Operators	Seitz form
$\hat{E}$	$\{1 \mid 0\}$
$\hat{R}_{2\alpha}$	$\{R_{2\alpha} \mid \frac{1}{2}(a_\alpha + a_\beta)\}$
$\hat{P}$	$\{-1 \mid 0\}$
$\hat{G}_\alpha$	$\{M_\alpha \mid \frac{1}{2}(a_\alpha + a_\beta)\}$

(3) There must exist another direction along which the component of $\vec{\tau}$ is nonzero. This can be deduced from the following. If all the other components of $\vec{\tau}$ (except for $\vec{\tau}_\alpha$) are zero, i.e., $\vec{\tau}_{n\alpha} = \vec{\tau} - \vec{\tau}_\alpha = 0$, we have $G_\alpha P = T_{2\vec{\tau}} P G_\alpha = T_{2\vec{\tau}_\alpha} P G_\alpha = e^{-i(2k_\alpha \tau_\alpha)} P G_\alpha = -P G_\alpha$ for four TRIMs in the $k_\alpha = \pi$ plane. Here $T_{2\vec{\tau}_\alpha}$ denotes an odd lattice translation with the amplitude of $2\tau_\alpha$ along the α direction. Thus, four TRIMs in the $k_\alpha = \pi$ plane are all fourfold degenerate with $g_\alpha = (+i, +i, -i, -i)$ in the quaternate bases $\{|\psi\rangle, PT|\psi\rangle, P|\psi\rangle, T|\psi\rangle\}$. We call this type of TRIMs in the $k_\alpha = \pi$ plane with $g_\alpha = (+i, +i, -i, -i)$ as "X"-type TRIMs. Band structures between two "X"-type TRIMs can be gapped, because the hourglass dispersion is no longer necessary to appear, such as the band connections shown in Fig. 2(a). As a result, there exists another direction along which the component of $\vec{\tau}$ possesses half-integer lattice translation, which gives another type of TRIMs with $g_\alpha = (+1, +1)$ or $g_\alpha = (-1, -1)$ in the bases of $\{|\psi\rangle, PT|\psi\rangle\}$. We call the two TRIMS with $g_\alpha = (+1, +1)$ or $g_\alpha = (-1, -1)$ in the bases of $\{|\psi\rangle, PT|\psi\rangle\}$ as "S" type TRIMs. Different from the "X"-type TRIMs, we find $[G_\alpha, P] = 0$ stands at the "S"-type TRIMs. Thus, G_α here must be a glide-mirror symmetry, while it cannot be a mirror symmetry.

(4) Given the three points above, there must exist two "X"-type TRIMs with $g_\alpha = (+i, +i, -i, -i)$ and two "S"-type TRIMs with $g_\alpha = (+1, +1)$ or $g_\alpha = (-1, -1)$. Given no other symmetries, the hourglass dispersion between "S"-type TRIM and "X"-type TRIM is not necessary to appear, such as the counter example shown in Fig. 2(b). Thus, another symmetry $\mathcal{R}$ is needed to introduce fourfold degeneracy with $g_\alpha = (+1, +1, +1, +1)$ or $g_\alpha = (-1, -1, -1, -1)$ at one "S"-type TRIM. Here, we call TRIMs with $g_\alpha = (+1, +1, +1, +1)$ or $g_\alpha = (-1, -1, -1, -1)$ as fourfold "S"-type TRIMs. $g_\alpha = (+1, +1, +1, +1)$ or $g_\alpha = (-1, -1, -1, -1)$ indicate that there exist two types of irreducible representations in which we have $D(G_\alpha) = I_{4\times4}$ or $D(G_\alpha) = -I_{4\times4}$ if some special quaternate bases are chosen. $D(G_\alpha)$ and $I_{4\times4}$ denote the representation matrix of G_α and the 4×4 identity matrix. It is clearly that $[D(G_\alpha), D(\mathcal{R})] \equiv 0$ stands in every irreducible representation, regardless of which type of irreducible representation it belongs to. Thus, the introduced symmetry $\mathcal{R}$ should satisfy the following conditions

$$[G_\alpha, \mathcal{R}] = 0\,,\ \{\mathcal{R}, P\} = 0 \tag{4}$$

at this fourfold "S"-type TRIM. $\{\mathcal{R}, P\} = 0$ is required by the following reasons. Firstly, it is known that either $\{\mathcal{R}, P\} = 0$ or $[\mathcal{R}, P] = 0$ stands at any TRIM. Since $P * \mathcal{R}$ and $\mathcal{R} * P$ always share the same rotation component in the real space, the difference between them must be an integer lattice translation $T_{\vec{\tau}}$. Thus, $\mathcal{R}P = T_{\vec{\tau}_r} P\mathcal{R} = e^{-i\vec{k}\cdot\vec{\tau}_r} P\mathcal{R} = \pm P\mathcal{R}$ stands when $\vec{k}$ is a $\mathcal{R}$-invariant TRIM for systems with symmetries $\mathcal{R}$ and P. $\vec{\tau}_r$ here denotes the translational vector of $T_{\vec{\tau}_r}$. As a result, $\{\mathcal{R}, P\} = 0$ or $[\mathcal{R}, P] = 0$ stands at arbitrary TRIMs. Furthermore, fourfold degeneracy can be induced only if $\{\mathcal{R}, P\} = 0$, while not $[\mathcal{R}, P] = 0$. In addition, $[G_\alpha, \mathcal{R}] = 0$ will constrain the fourfold degeneracy with $D(G_\alpha) = I_{4\times4}$ or $D(G_\alpha) = -I_{4\times4}$ in the quaternate bases $\{|\psi\rangle, PT|\psi\rangle, \mathcal{R}|\psi\rangle, \mathcal{R}PT|\psi\rangle\}$.

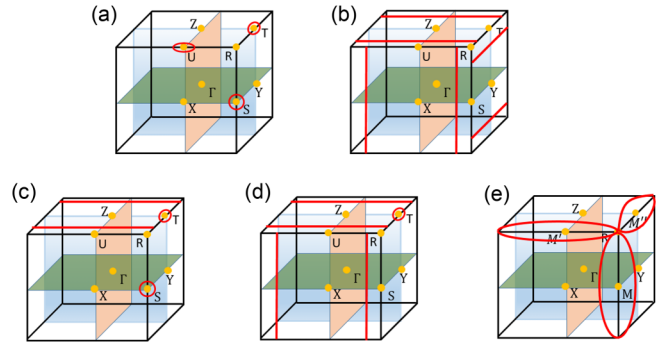

FIG. 6. (a)–(d) The schematic figures for the configurations of FEDLs in SG.61 in the BZ. We have neglected the possible connections of different FEDLs for simplicity. From Fig. 6(a) to Fig. 6(b), the FEDL encircling S/T/U in the $k_x = \pi/k_y = \pi/k_z = \pi$ plane becomes two Dirac nodal loops crossing the $k_x = \pi/k_y = \pi/k_z = \pi$ plane, respectively. Similarly, the FEDL encircling U in the $k_z = \pi$ plane becomes two Dirac nodal loops crossing the $k_z = \pi$ plane in Fig. 6(c), while the FEDL encircling S/U in the $k_x = \pi/k_z = \pi$ plane becomes two Dirac nodal loops crossing the $k_x = \pi/k_z = \pi$ plane in Fig. 6(d). (a),(b),(e) The schematic figures for the configurations of FEDLs in SG.205 in the BZ.

Equivalently, Eq. (4) can be written as

$$[G_\alpha, \mathcal{M}] = 0\,,\ \{\mathcal{M}, P\} = 0 \tag{5}$$

with $\mathcal{M} = \mathcal{R}P$. It can be deduced in the following. Firstly, we have $[G_\alpha, \mathcal{M}] = [G_\alpha, \mathcal{R}P] = [G_\alpha, \mathcal{R}]P + \mathcal{R}[G_\alpha, P] = 0$. Here we have used $[G_\alpha, \mathcal{R}] = 0$ in Eq. (4), and $[G_\alpha, P] = 0$ is required by "S"-type TRIMs. Secondly, we have $\{\mathcal{M}, P\} = \{\mathcal{R}P, P\} = \mathcal{R}PP + P\mathcal{R}P = \mathcal{R} + (-\mathcal{R}P)P = \mathcal{R} - \mathcal{R} = 0$.

Given all these conditions above, hourglass Dirac dispersion protected by the G_α between fourfold "S"-type TRIM and "X"-type TRIM is constructed. Furthermore, nodal phenomena protected by some glide-mirror symmetry must be a one-dimensional nodal loop. Thus, the Dirac nodal loop is induced.

B. SGs hosting FEDLs

In the following, we will deduce all SGs hosting FEDLs in the nonmagnetic systems. In terms of any symmetry A, it acts on both the real space and the spin space. When we focus our discussion on the real space, we use $\hat{A}$ instead of the symmetry A. Then, the expression of $\mathcal{R}$ in the real space (denoted by $\hat{\mathcal{R}}$) is the key for us to deduce all SGs possessing FEDLs. For systems with the inversion symmetry, $\hat{\mathcal{R}}$ can be chosen as two/three/four/sixfold rotation (or screw rotation). The corresponding point groups of SGs containing $\hat{G}_\alpha$, $\hat{P}$, and $\hat{\mathcal{R}}$ must belong to $\{D_{2h}, D_{4h}, D_{3d}, D_{6h}, T_h, O_h\}$. $[G_\alpha, \mathcal{R}] = 0$ in Eq. (4) requires $[\hat{G}_\alpha, \hat{\mathcal{R}}] = 0$ in the real space. After enumerating these point groups one by one, we find the commutation

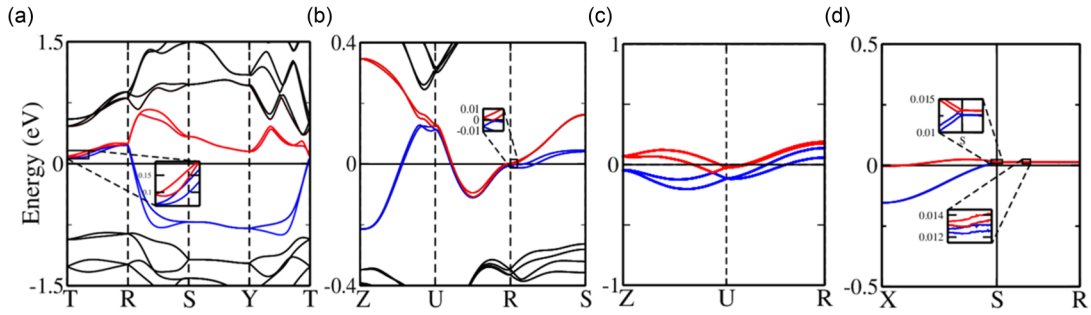

FIG. 7. Band structures of (a) K_2SnBi in SG.57, (b) $Hf_2Co3Si4$ in SG.60, (c) AgF_2 in SG.61, and (d) $AgAsF_7$ in SG.62, respectively. The insets in them show us the hourglass dispersions protected by the corresponding glide-mirror symmetries in SG.57, SG.60, SG.61, and SG.62, respectively.

relation $[\hat{G}_\alpha, \hat{\mathcal{R}}] = 0$ in the real space (up to some integer lattice translation) requires that $\hat{\mathcal{R}}$ must be either the twofold rotation (or screw rotation) orthogonal to the α direction, or the two/three/four/six-fold rotation (or screw rotation) along the α direction. Firstly, we will prove that $\hat{\mathcal{R}}$ cannot be two/three/four/six-fold rotation (or screw rotation) along the α direction. If $\hat{\mathcal{R}}$ is some rotation (or screw rotation) along the α direction, we have $[\mathcal{R}, R_{2\alpha}] = [\mathcal{R}, G_\alpha P] = 0$. Here $R_{2\alpha} = G_\alpha P$ denotes the two-fold screw rotation along the α direction. Using the anticommutation relation $\{\mathcal{R}, P\} = 0$ at the fourfold "S"-type TRIM, we have

$$\begin{aligned} G_\alpha \mathcal{R} &= R_{2\alpha} P \mathcal{R} \\ &= R_{2\alpha}(-\mathcal{R}P) \\ &= -R_{2\alpha}\mathcal{R}P \\ &= -\mathcal{R}R_{2\alpha}P \\ &= -\mathcal{R}G_\alpha. \end{aligned} \tag{6}$$

Equation (6) contradicts with the commutation relation $[G_\alpha, \mathcal{R}] = 0$ at the fourfold "S"-type TRIM. As a result, $\hat{\mathcal{R}}$ cannot be two/three/four/sixfold rotation (or screw rotation) along the α direction. Thus, $\hat{\mathcal{R}}$ must be some twofold rotation (or screw rotation) orthogonal to the α direction. Then, $\hat{\mathcal{R}}$ can be denoted by $\hat{R}_{2\beta}$ with the β direction orthogonal to the α direction, the corresponding point groups of SGs containing $\hat{G}_\alpha$, $\hat{P}$, and $\hat{\mathcal{R}}$ must be either D_{2h} or supergroups of D_{2h}. Let us focus on SGs with D_{2h} point group first. We choose the inversion center as the origin, the α and β directions are along the x axis and y axis, respectively. According to the discussions above, we know that τ_α and some other component of $\vec{\tau}$ must be $\frac{1}{2}$, while the third component of $\vec{\tau}$ can be either 0 or $\frac{1}{2}$. In terms of $G_\beta = \{m_\beta|\vec{\tau}'\}$, we do not give any direct constraint of $\vec{\tau}'$, but the introduced G_β must be compatible with Eq. (5) at fourfold "S"-type TRIMs. Then the Seitz notations of the inversion symmetry, $\hat{G}_\alpha$ and $\hat{G}_\beta$, as generators in the real space can be expressed in Table I.

Firstly, we choose $\hat{G}_\alpha = \{m_{100}|\frac{1}{2}\frac{1}{2}0\}$ to show how we can get SGs possessing fourfold "S"-type TRIMs. In this case, we can easily find $X : (\pi, 0, 0)$ and $U : (\pi, 0, \pi)$ are "X"-type TRIMs, while $S : (\pi, \pi, 0)$ and $R : (\pi, \pi, \pi)$ are "S"-type TRIMs. $\hat{G}_\beta$ can be expressed as $\hat{G}_\beta = \{m_{010}|lmm\}$, with $l, m, n \in \{0, \frac{1}{2}\}$. We find $G_\alpha G_\beta = \bar{E}T_{-2l,1,0}G_\beta G_\alpha$. Here, $\bar{E}$ comes from the anticommutation relation $m_{100}m_{010} = \bar{E}m_{010}m_{100}$ in the spin space. Then, we have $[G_\alpha, G_\beta] = 0$ at S and R if $l = 0$, while $\{G_\alpha, G_\beta\} = 0$ at S and R if $l = \frac{1}{2}$. As the first equation (i.e., $[G_\alpha, \mathcal{M}] = 0$) required in Eq. (5), fourfold "S"-type TRIMs can appear if $l = 0$. In the following, we will focus on the second equation (i.e., $\{\mathcal{M}, P\} = 0$) required in Eq. (5) at fourfold "S"-type TRIMs when $l = 0$. We find $G_\beta P = T_{2l,2m,2n}PG_\beta$, thus,

(1) if $l = m = n = 0$, we have $G_\beta P = PG_\beta$ which is not in accordance with the anticommutation relation required in Eq. (5). In this case, there is no fourfold "S"-type TRIM and FEDL.

(2) if $l = 0, m = \frac{1}{2}, n = 0$, we have $G_\beta P = -PG_\beta$ at both S and R, which is in accordance with the anticommutation relation required in Eq. (5). In this case, both the S and R TRIMs are fourfold "S"-type TRIMs. There must be two FEDLs in $k_\alpha = \pi$ plane. After some coordinate transformation, we find the corresponding SG is SG.57.

(3) if $l = 0, m = 0, n = \frac{1}{2}$, $G_\beta P = -PG_\beta$ stands at R, which is in accordance with the anticommutation relation required in Eq. (5). In this case, the R TRIM is the unique fourfold "S"-type TRIM and there must be a FEDL in $k_\alpha = \pi$ plane. After some coordinate transformation, we find the corresponding SG is SG.60.

(4) if $l = 0, m = \frac{1}{2}, n = \frac{1}{2}$, $G_\beta P = -PG_\beta$ stands at S, which is in accordance with the anticommutation relation required in Eq. (5). In this case, the S TRIM is the unique fourfold "S"-type TRIM and there must be a FEDL in the $k_\alpha = \pi$ plane. After some coordinate transformation, we find the corresponding SG is SG.61.

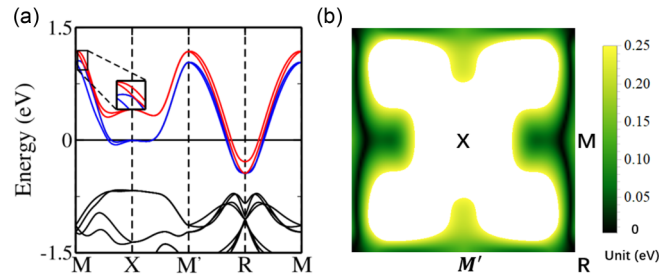

FIG. 8. (a) Band structures of IrN_2 in SG.205. (b) Illustration figure of the direct gap between the minimum conduction band and the maximum valence band near the Fermi level on the $k_x = \pi$ plane. We choose 0.25 eV as the energy cut, i.e., zone with energy gap larger than 0.25 eV is represented with the white color.

TABLE III. The symmetry-breaking transitions of SG.57.

SG.57-sg.n	Filling factor of sg.n	Coordinate transformation	Phase transition
sg.11	4n	$\{a,b,c\}_{sg.11}=\{b,c,a\}_{SG.57}$	{FEDLCBZs, FEDLTBZs}→ I
sg.13	4n	$\{a,b,c\}_{sg.13}=\{c,a,b\}_{SG.57}$	{FEDLCBZs, FEDLTBZs}→ {$2\mathcal{DP}\oplus 2\mathcal{DP}$, I}
sg.14	4n		{FEDLCBZs, FEDLTBZs}→ {DNLCBZs, DNLTBZs}
sg.18	4n	$\{a,b,c\}_{sg.18}=\{b,c,a\}_{SG.57}$	{FEDLCBZs, FEDLTBZs}→ { $2\mathcal{DN}\oplus 2\mathcal{DN}$, I}
sg.26	4n	$\{a,b,c\}_{sg.26}=\{c,a,b\}_{SG.57}$	FEDLs → I
sg.28	4n	$\{a,b,c\}_{sg.28}=\{c,b,-a\}_{SG.57}$	{FEDLCBZs, FEDLTBZs}→{4 CWNLs, 4 WNLTBZs}
sg.29	8n	$\{a,b,c\}_{sg.29}=\{-b,a,c\}_{SG.57}$	{FEDLCBZs, FEDLTBZs}→{2 CWNCs, 4 WNLTBZs}

1. The "Filling factor of sg.n" column denotes the filling that realizes a band insulator for the subgroup sg.n.
2. FEDLCBZs and FEDLTBZs denote the contractible/noncontractible FEDLs, respectively. Similarly, DNLCBZs and DNLTBZs represent Dirac nodal loops which are contractible and noncontractible in the BZ, respectively.
3. $2\mathcal{DP}\oplus 2\mathcal{DP}$ and $2\mathcal{DN}\oplus 2\mathcal{DN}$ mean two Dirac points and two DNs along the R-T line are possible to exist when each separated FEDL is protected by R_{2x} symmetry. DN here represents a fourfold degenerate node along R-T, with its dispersions doubly degenerate in the $k_y=\pi$ and $k_z=\pi$ planes, while without degeneracy along the other directions.
4. I, CWNL, WNLTBZ, and CWNC denote insulator, concentric Weyl nodal loop, Weyl nodal loops traversing the BZ, and concentric Weyl nodal chain, respectively.
5. Here "$A\oplus B$" indicates nodal phenomena A and B are independent with each other, and can be obtained simultaneously.

Secondly, in terms of the other case $\hat{G}_\alpha=\{m_{100}|\frac{1}{2}\frac{1}{2}\frac{1}{2}\}$, we can easily find $X:(\pi,0,0)$ and $R:(\pi,\pi,\pi)$ are "X"-type TRIMs, while $S:(\pi,\pi,0)$ and $U:(\pi,0,\pi)$ are "S"-type TRIMs. We find $G_\alpha G_\beta=\bar{E}T_{-2l,1,0}G_\beta G_\alpha$ also stands in this case. Then, we have $[G_\alpha,G_\beta]=0$ at S when $l=0$, while $[G_\alpha,G_\beta]=0$ at U when $l=\frac{1}{2}$. As the first equation (i.e., $[G_\alpha,\mathcal{M}]=0$) required in Eq. (5), the S TRIM can be the fourfold "S"-type TRIM if $l=0$, while the U TRIM can be the fourfold "S"-type TRIM if $l=\frac{1}{2}$. In the following, we will focus on the second equation (i.e., $\{\mathcal{M},P\}=0$) required in Eq. (5) at fourfold "S"-type TRIMs for the cases of $l=0$ and $l=1$, respectively. In terms of $l=0$,

(1) if $(l,m,n)\in\{(000),(00\frac{1}{2})\}$, we have $[G_\beta,P]=0$ stands at S, which is not in accordance with the anticommutation relation required in Eq. (5). Thus, there is no fourfold "S"-type TRIM and FEDL.

(2) if $(l,m,n)\in\{(0\frac{1}{2}0),(0\frac{1}{2}\frac{1}{2})\}$, we have $\{G_\beta,P\}=0$ stands at S, which is in accordance with the anticommutation relation required in Eq. (5). Thus, the S TRIM is the fourfold "S"-type TRIM, which indicates there exists a FEDL in this case. After some coordinate transformation, we find the corresponding SGs are SG.60 and SG.62.

Similarly, in terms of $l=\frac{1}{2}$,

(1) if $(l,m,n)\in\{(\frac{1}{2}0\frac{1}{2}),(\frac{1}{2}\frac{1}{2}\frac{1}{2})\}$, we have $[G_\beta,P]=0$ stands at U, which is not in accordance with the anticommutation relation required in Eq. (5). Thus, there is no fourfold "S"-type TRIM and FEDL.

(2) if $(l,m,n)\in\{(\frac{1}{2}00),(\frac{1}{2}\frac{1}{2}0)\}$, we have $\{G_\beta,P\}=0$ stands at U, which is in accordance with the anticommutation relation required in Eq. (5). Thus, the U TRIM is the fourfold "S"-type TRIM, which indicates there exists a FEDL in this case. After some coordinate transformation, we find the corresponding SGs are SG.62 and SG.60.

Thus, after enumerating all the possibilities of the concrete forms of $\hat{G}_\alpha$ and $\hat{G}_\beta$, we find there are only four SGs possessing the fourfold "S"-type TRIMs (which lead to the FEDLs), they are SG.57, SG.60, SG.61 and SG.62, respectively.

It is well known that any symmetry in a subgroup will be preserved in all the corresponding supergroups. Thus, all supergroups of SG.57, SG.60, SG.61 and SG.62 can also possess the FEDLs at the first sight. But, it is not the story indeed. Let us choose SG.61 as an example to illuminate this. SG.73 is a supergroup of SG.61 with the corresponding coset representative $\{E,T_{\frac{1}{2}\frac{1}{2}\frac{1}{2}}\}$. For body-centered systems,

TABLE IV. The symmetry-breaking transitions of SG.60.

SG.60-sg.n	Filling factor of sg.n	Coordinate transformation	Phase transition
sg.13	4n		{SFEDL, FEDC}→ {4 DPs, I}
sg.14-class a	4n	$\{a,b,c\}_{sg.14}=\{c,a,b\}_{SG.60}$	{SFEDL, FEDC}→ DNLx
sg.14-class b	4n	$\{a,b,c\}_{sg.14}=\{a,c,-a-b\}_{SG.60}$	{SFEDL, FEDC}→ DNLz
sg.18	4n	$\{a,b,c\}_{sg.18}=\{c,a,b\}_{SG.60}$	{SFEDL, FEDC}→ {4 DNs, I}
sg.29	8n	$\{a,b,c\}_{sg.29}=\{-b,a,c\}_{SG.60}$	{SFEDL, FEDC}→ CWNCx
sg.30	4n	$\{a,b,c\}_{sg.30}=\{c,a,b\}_{SG.60}$	{SFEDL, FEDC}→ {2 CWNLs, WNN}
sg.33	8n	$\{a,b,c\}_{sg.33}=\{c,b,-a\}_{SG.60}$	{SFEDL, FEDC}→ CWNCz

1. SFEDLs/FEDC means the FEDLs in SG.60 are composed of two separated FEDLs or only one Dirac nodal chain, respectively.
2. DNLx/DNLz denotes Dirac nodal loop in the $k_x=\pi/k_z=\pi$ plane, which will be reserved under SG.60-sg.14-class a/b transition, respectively.
3. CWNCx and CWNCz denote concentric Weyl nodal chain in the $k_x=\pi$ and $k_z=\pi$ plane, respectively, while WNN denotes the Weyl nodal net schematized in Fig. 9(c).

TABLE V. The symmetry-breaking transitions of SG.61.

SG.61-sg.n	Filling factor of sg.n	Phase transition
sg.14-class β	4n	FEDL $\rightarrow$ DNL$\beta \oplus 2\mathcal{DP}\gamma \oplus 2\mathcal{DP}\alpha$
sg.19	4n	FEDL $\rightarrow$ $2\mathcal{DN}x \oplus 2\mathcal{DN}y \oplus 2\mathcal{DN}z$
sg.29-class β	8n	FEDL $\rightarrow$ CWNCα/WNLTBZα $\oplus$ CWNLγ/WNCTBZγ

1. $2\mathcal{DP}\gamma$ and $2\mathcal{DP}\alpha$ mean that two DPs along the $k_\alpha = \pi \cap k_\gamma = \pi$ line are possible to exist when some FEDL protected by $R_{2\beta}$ symmetry crosses this line.
2. Similarly, $2\mathcal{DN}\alpha$ ($\alpha \in \{x, y, z\}$) indicates that 2 DNs are possible to exist when the contractible/noncontractible FEDL in the $k_\alpha = \pi$ plane is simultaneously protected by $R_{2\gamma}/R_{2\beta}$ symmetry.
3. In the case of SG.61-sg.29-class β transition, CWNCα and WNLTBZα are short for concentric Weyl nodal chain and Weyl nodal loop noncontractible in the $k_\alpha = \pi$ plane, while CWNLγ and WNCTBZγ are short for concentric Weyl nodal loop and Weyl nodal chain noncontractible in the $k_\gamma = \pi$ plane, respectively. "$A \oplus B$" indicates nodal phenomena A and B are independent with each other, and can be available simultaneously, while "A/B" indicates nodal phenomena A and B are alternative under some transition. Figure 10 shows how the FEDLs evolve under SG.61-sg.29-class β transition.

$k_\alpha = 0$ plane is the only G_α invariant plane. Thus, the FEDL defined in the $k_\alpha = \pi$ plane does not exist in this supergroup (SG.73). We remind the readers that all our discussions and derivations about $\hat{G}_\alpha$ and $\hat{G}_\beta$ to deduce the FEDLs are based on the primitive lattice vectors, i.e., the zero and nonzero components of $\vec{\tau}$ and $\vec{\tau}'$ in $\hat{G}_\alpha$ and $\hat{G}_\beta$ are in the unit of the primitive lattice vectors. If these components change under the primitive lattice vectors of corresponding supergroups, the discussions and deductions above will no longer stand and the FEDLs will disappear. In terms of the supergroup SG.73 (of subgroup SG.61), we find the primitive lattice vectors of the subgroup SG.61 are different from that of the supergroup SG.73. This difference leads to different expressions of $\vec{\tau}$ and $\vec{\tau}'$ in $\hat{G}_\alpha$ and $\hat{G}_\beta$ in the supergroup SG.73, thus, the FEDLs disappear in the supergroup. After enumerating all supergroups of SG.57, SG.60, SG.61, and SG.62 with $\vec{\tau}$ and $\vec{\tau}'$ in $\hat{G}_\alpha$ and $\hat{G}_\beta$ unchanged in the bases of the corresponding primitive lattice vectors, we find SG.205 is another SG, and the only supergroup, possessing FEDLs.

As a result, there exist five and only five SGs satisfying these conditions above, namely, SG.57, SG.60, SG.61, SG.62 and SG.205. Furthermore, we find that the fillings which realize a band insulator for all these groups are $8n$, and the Dirac nodal loop comes from the band crossings between PT related doublets $8n + 3 \oplus 8n + 4$ and PT related doublets $8n + 5 \oplus 8n + 6$, suggesting these Dirac nodal loops appear at the Fermi level when systems of these SGs are half-filled. Here $(8n + 3) \oplus (8n + 4)$ doublet is the PT related doublet composed of the $(8n + 3)$th and $(8n + 4)$th bands according to the order of energy. As a result, we call these systems FEDL materials.

C. Configurations of FEDLs in SG.57,60,61,62,205

In the following, we focus on the configurations of the FEDLs in all these SGs, among which SG.60 [83], SG.61 [86] and SG.62 [84,85] have been proposed in the earlier works. According to the above discussion, we deduce the schematic figures of all the FEDLs for the five SGs, as shown in Fig. 3. Here we have chosen the cases that all the Dirac nodal loops are separated and contractible in the BZ for simplicity in the figure. The words "contractible in the BZ" ("noncontractible in the BZ") mean that the Dirac nodal loop can (cannot) be compressed to an infinitesimal Dirac nodal loop surrounding the fourfold "S"-type TRIM. If some FEDL is noncontractible in the BZ, it means that this FEDL cannot be translated into the first BZ without touching any boundary of the BZ. Thus, the noncontractible FEDL is no other than the FEDL traversing the BZ. Fig. 3 shows the FEDLs separated and contractible in the BZ. However, FEDLs in each SG can touch each other and can be noncontractible in the BZ [83,86]. It is natural for us to explore all the possible configurations of the FEDLs.

1. Configurations of FEDLs in SG.57

As shown in Figs. 4(a) and 4(c), there are two different configurations of FEDLs in the $k_y = \pi$ plane in SG.57, named as contractible FEDLs and noncontractible FEDLs in the BZ. The corresponding connections of the bands satisfying the

TABLE VI. The symmetry-breaking transitions of SG.62.

SG.62-sg.n	Filling factor of sg.n	Coordinate transformation	Phase transition
sg.11	4n		CFEDL $\rightarrow$ I
sg.14-class a	4n	$\{a, b, c\}_{sg.14} = \{-b, a, b + c\}_{SG.62}$	FEDL $\rightarrow$ DNL
sg.14-class b	4n	$\{a, b, c\}_{sg.14} = \{b, c, a\}_{SG.62}$	FEDL $\rightarrow$ $2\mathcal{DP}$s
sg.19	8n		FEDL $\rightarrow$ 2 $\mathcal{DN}$s
sg.26	4n	$\{a, b, c\}_{sg.26} = \{b, c, a\}_{SG.62}$	FEDL $\rightarrow$ I
sg.31	4n	$\{a, b, c\}_{sg.31} = \{-b, a, c\}_{SG.62}$	FEDL $\rightarrow$ CDNL
sg.33	8n	$\{a, b, c\}_{sg.33} = \{a, -c, b\}_{SG.62}$	FEDL $\rightarrow$ CDNC

1. If the two crossing points of FEDL along R-S are protected by R_{2z}, two DPs/DNs (denoted by $2\mathcal{DP}$s/$2\mathcal{DN}$s) appear under SG.62-sg. 14-class b/SG.62-sg.19 transition, respectively.

TABLE VII. The symmetry-breaking transitions of SG.205.

SG.205-sg.n	Filling factor of sg.n	Phase transition
sg.61	8n	{CFEDLs,FEDLTBZs,DNN} → {CFEDLs,FEDLTBZs,AFEDLs}
sg.148	2n	{CFEDLs,FEDLTBZs,DNN} → I
sg.198	8n	{CFEDLs,FEDLTBZs,DNN} → {6$\mathcal{DN}$s, 6$\mathcal{DN}$s,I}

1. CFEDLs/FEDLTBZs indicate that the FEDLs are contractible/noncontractible in the BZ, respectively, while DNN represents the Dirac nodal net schematized in Fig. 6(e). AFEDLs indicate the DNN can be tuned to arbitrary configuration of FEDLs in SG.6 under SG.205-sg.61 transition.
2. 6$\mathcal{DN}$s indicate that six fourfold DNs related with each other by $R_{3[111]}$ symmetry may appear at three $R_{2\alpha}$ invariant lines, S-R, T-R, and U-R, respectively, when the FEDLs are protected by the $R_{2\alpha}$ symmetries. Otherwise, these FEDLs will be gapped. Even though the FEDLs may be gapped under the SG.205-sg.198 transition, the filling that realizes a band insulator remains unchanged to be $8n$, which indicates the system is still half filled and semimetallic.

compatibility relations are shown in Figs. 4(b) and 4(d), respectively. According to the compatibility relation along R-T, we emphasize here that Dirac nodal chain (a Dirac nodal chain is an one-dimensional nodal configuration which is composed of two Dirac nodal loops touching with each other at some isolate point in the BZ) composed of the two FEDLs touching at some isolated point along R-T is prohibited.

2. *Configurations of FEDLs in SG.60*

There are two FEDLs in SG.60, with one lying in $k_x = \pi$ plane, while the other lying in $k_z = \pi$ plane. They are protected by G_x and G_z, respectively.

To obtain some intuitive pictures, we list several possible band connections according with the compatibility relation along U-R, which gives a Dirac nodal chain from Figs. 5(a)–(c), and two separated FEDLs from Figs. 5(d) and 5(e), respectively. Reminding of the earlier work [69], one may consider a third configuration of the FEDLs, i.e., the Dirac nodal links. A Dirac nodal link is a one-dimensional nodal configuration which is composed of two Dirac nodal loops locked with each other. The hypothetical Dirac nodal link appears when these two separated FEDLs go close, and then cross with each other. Thus, the crossing point of the Dirac nodal link near R is protected by G_z, while the crossing point near U is protected by G_x. Band crossings protected by G_z can only come from bands between $\bar{P}_2\bar{P}_2(2)(\bar{P}_4\bar{P}_4(2))$ and $\bar{P}_3\bar{P}_3(2)(\bar{P}_5\bar{P}_5(2))$, where $\bar{P}_i$ is an irreducible representation of the little group at P. The notation can be looked up on the Bilbao Crystallographic Server [96,97]. However, both bands $\bar{P}_2\bar{P}_2(2)(\bar{P}_4\bar{P}_4(2))$ and $\bar{P}_3\bar{P}_3(2)(\bar{P}_5\bar{P}_5(2))$ are simultaneously valence bands or conductance bands, as a result, Dirac nodal link can be obtained by bands below or above the Fermi level, while cannot be obtained by bands between $8n+3 \oplus 8n+4$ doublet and $8n+5 \oplus 8n+6$ doublet at the Fermi level.

In addition, the Dirac nodal loop encircling R in the $k_x = \pi$ plane is either contractible or noncontractible in the BZ along the k_z axis. We define a new ζ_2 index as

$$\zeta_2 = \frac{n_+(S) - n_+(R)}{2} \bmod 2 \tag{7}$$

to tell whether this Dirac nodal loop is contractible in the BZ or not. In Eq. (7), $n_+(R)$ and $n_+(S)$ represent the number of occupied bands with $+1$ G_x eigenvalue at R and S, respectively. $\zeta_2 = 0$ indicates that this Dirac nodal loop is noncontractible in the BZ, while $\zeta_2 = 1$ indicates this Dirac nodal loop is contractible in the BZ. This new ζ_2 index can be obtained as follows. Let us focus on the FEDL in the $k_x = \pi$ plane. Suppose this FEDL is contractible in the BZ, it means that there exists a band crossing (originating from this FEDL) between bands with the opposite G_x eigenvalues along R-S. This band crossing will change the order of the bands near the crossing point, making the number of the occupied bands with $g_x = +1$ at R larger/smaller than that at S by 2, i.e., $n_+(R) - n_+(S) = \pm 2$, which gives $\zeta_2 = 1$. In the contrary, if this FEDL is noncontractible in the BZ, it means there is no band crossing between bands with the opposite G_x eigenvalues along R-S. Thus, $n_+(R) - n_+(S) = 0$, which gives $\zeta_2 = 0$. We also remind that we have neglected the existence of an occasional Dirac nodal loop. If bands with the opposite G_x eigenvalues near the Fermi level cross twice along R-S, it also gives $\zeta_2 = 0$. In this case, there exists another occasional Dirac nodal loop encircling the FEDL in the $k_x = \pi$ plane.

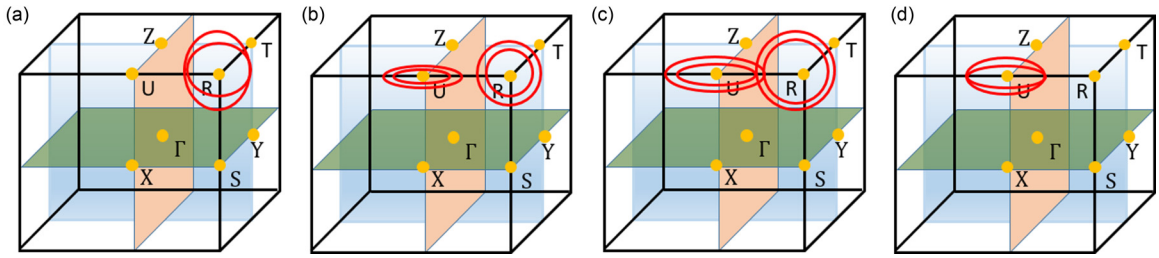

FIG. 9. The evolution of FEDLs in SG.60 under (a) SG.60-sg.29, (b),(c) SG.60-sg.30, and (d) SG.60-sg.33 transitions. The red loops denote how the FEDLs split under these transitions. We remind the readers that the Weyl nodal loops surrounding U are in the $k_z = \pi$ plane, while those surrounding R are in the $k_x = \pi$ plane.

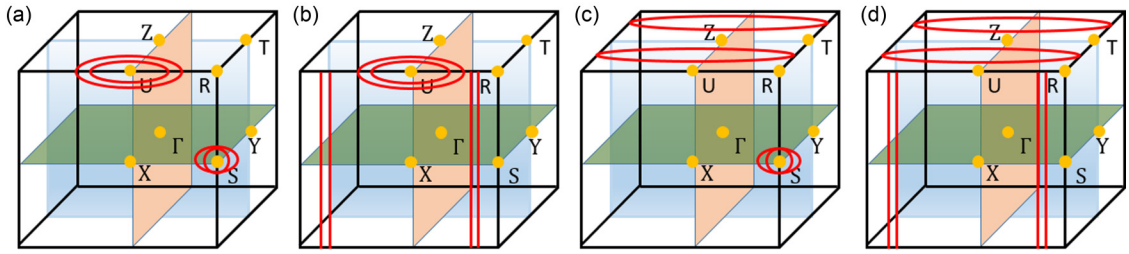

FIG. 10. The evolution of the FEDLs in SG.61 under SG.61-sg.29-class b transition. We remind the readers that the Weyl nodal loops surrounding S and U in Figs. 10(a)–10(c) are in the $k_x = \pi$ plane and $k_z = \pi$ plane, respectively.

3. Configurations of FEDLs in SG.61

SG.61 contains three screw axes, the inversion, and three glide mirrors, as shown in Table II. The subscripts satisfy $(\alpha, \beta) = \{(x, y); (y, z); (z, x)\}$, which presents a cyclic permutation relation. As a result, there exists a FEDL on each surface of the BZ surrounding S, T, and U, respectively. Similar with the FEDL in the $k_x = \pi$ plane of SG.60, each FEDL of SG.61 can be either contractible or noncontractible in the BZ, which can also be distinguished by three $(\zeta_{2x}, \zeta_{2y}, \zeta_{2z})$ indexes

$$\zeta_{2x} = \frac{n^x_+(S) - n^x_+(R)}{2} \bmod 2,$$
$$\zeta_{2y} = \frac{n^y_+(T) - n^y_+(R)}{2} \bmod 2,$$
$$\zeta_{2z} = \frac{n^z_+(U) - n^z_+(R)}{2} \bmod 2. \tag{8}$$

In Eq. (8), $n^x_+(S)/n^y_+(T)/n^z_+(U)$ and $n^{x/y/z}_+(R)$ represent the numbers of occupied bands with $+1$ $G_{x/y/z}$ eigenvalue at $S/T/U$ and R, respectively. $\zeta_{2\alpha} = 0$ indicates the Dirac nodal loop in the $k_\alpha = \pi$ plane is noncontractible in the BZ, while $\zeta_{2\alpha} = 1$ indicates this Dirac nodal loop is contractible in the BZ. As a result, FEDLs shown in Figs. 6(a), 6(b) 6(c), and 6(d) indicate the corresponding $\{\zeta_{2x}, \zeta_{2y}, \zeta_{2z}\}$ equals $\{1, 1, 1\}$, $\{0, 0, 0\}$, $\{1, 1, 0\}$, and $\{1, 0, 0\}$, respectively.

It should be noted that when $\{\zeta_{2\alpha}, \zeta_{2\beta}\} = \{0, 1\}$ for some system, the Dirac nodal loops in the $k_\alpha = \pi$ and $k_\beta = \pi$ planes may touch each other, and thus, a Dirac nodal chain forms, such as the AgF_2 system in SG.61 [86].

4. Configurations of FEDLs in SG.62

There is only one FEDL in the $k_x = \pi$ plane, and it must be contractible in the BZ because there is only one four-dimensional irreducible representation along X-U-R of SG.62. Thus, bands between $8n + 3 \oplus 8n + 4$ doublet and $8n + 5 \oplus 8n + 6$ doublet must be gapped along X-U-R, leading the FEDL contractible in the BZ.

5. Configurations of FEDLs in SG.205

SG.205 can be seen as a cubic case of SG.61 as a result of SG.205 = SG.61 $\otimes R_{3[111]}$. $R_{3[111]}$ denotes the threefold rotation along the body-diagonal direction. Thus, these three FEDLs are simultaneously either contractible in the BZ or noncontractible in the BZ and related to each other by the $R_{3[111]}$ symmetry, as shown in Figs. 6(a) and 6(b), respectively. More interestingly, we find that the separated FEDLs may meet with each other at R, as schematized in Fig. 6(e). In this case, this special FEDL at R is sixfold degenerate [77].

Similar with SG.60 and SG.61, we can introduce $\zeta_2 = \zeta_{2x} = \zeta_{2y} = \zeta_{2z}$ as

$$\zeta_2 = \frac{n^x_+(M) - n^x_+(R)}{2} \bmod 2 \tag{9}$$

to distinguish the three different configurations in SG.205. $\zeta_2 = 1$ indicates that the three FEDLs are contractible in the BZ, while $\zeta_2 = 0$ indicates the three FEDLs are noncontractible in the BZ or just connect with each other at R. To further identify whether the FEDLs are composed of three separated Dirac nodal loops noncontractible in the BZ or connected with each other at R when $\zeta_2 = 0$, more calculations along M-R are needed. In the following, we will use IrN_2 as an example to illustrate this.

To justify the FEDLs in each SG, we calculate band structures of K_2SnBi in SG.57, $Hf_2Co_3Si_4$ in SG.60, AgF_2 in SG.61, $AgAsF_7$ in SG.62, and IrN_2 in SG.205, as shown in Figs. 7(a)–7(d) and Figs. 8(a) and 8(b), respectively. We can see the hourglass dispersions protected by the corresponding glide-mirror symmetry from the band structures in each SG, which indicates they are indeed FEDL materials. Especially for the case of $Pa\bar{3}$ IrN_2, the FEDL lies close to M-R and touches this line at R, as the black line shows in Fig. 8(b). It

TABLE VIII. FEDL materials in SG.57.

Materials	Materials	Materials	Materials
Cs(C;100,1)	$Pr_3(GaNi)_2$(C;000,2)	ReN_2(C;000,3)	$YbCrSb_3$(C;000,3)
K_2SnBi(C;000,0)	$Pr_3(GeRu)_2$(C;000,1)	K_5Hg_7(C;000,0)	ThTl(T;000,1)
CaAlPd(C;100,2)	$La_3(GaNi)_2$(C;100,1)	HfGa(C;000,1)	$Na_8In_6Au_{11}$(C;000,3)
Ca_4MgAl_3(C;000,1)	$Y_3(SiRh)_2$(C;000,1)		

1. C/T indicates the configuration of the FEDLs in SG.57 is composed by two contractible/noncontractible FEDLs in the BZ, respectively.

TABLE IX. FEDL materials in SG.60.

Materials	Materials	Materials	Materials
Fe_2N(S;C;110,0)	ReO_2(C;C;110,2)	$RbCuCl_3$(C;C;110,2)	Al_3FeSi_2(S;C;110,3)
Mn_2N(S;C;110,3)	$Si_2Ni_7P_5$(C;C;110,1)	$Hf_2Co_3Si_4$(C;C;110,3)	

1. S/C means that the FEDLs are composed by two separated Dirac nodal loops or only one Dirac nodal chain, while C/T indicates the FEDL in the $k_x = \pi$ plane is contractible or noncontractible in the BZ, respectively.

means that the corresponding FEDL is no other than the Dirac nodal net, as schematized in Fig. 6(e).

IV. EVOLUTIONS OF FEDLS UNDER SYMMETRY-BREAKING BUT TRANSLATION-INVARIANT TRANSITIONS

In the above, we have deduced all possible configurations of the FEDLs in the five SGs and classify them accordingly. Furthermore, it is well known that perturbations like strains, external magnetic fields, circularly polarized lights, and so on, can serve as useful methods to tune the band structures in condensed matter systems. Generally, these perturbations will break some symmetries, and then, how the FEDLs in the five SGs evolve under these perturbations remains a question. In the following, we will explore the evolutions of these FEDLs under maximal-subgroup symmetry-breaking transitions which respect the translation symmetries. Suppose all the transitions are obtained by the adiabatic perturbations, which indicates that no new band crossings occur in this progress. Furthermore, it should be noted that we have neglected what and how the perturbations are applied to get the corresponding transitions.

Firstly, taking SG.57 as an example, we can get all types of symmetry-breaking transitions of SG.57 from the Bilbao Crystallographic Server. We denote the transition as SG.57-sg.n, where "sg.n" denotes some maximal subgroup of SG.57 with k index = 1 (k index = 1 indicates that the corresponding transition does not break any translation symmetry). If the FEDL crosses the R-T line, band crossings from the FEDL along this line must be simultaneously protected by either the R_{2x} or the G_z symmetry (besides the G_y symmetry) from the compatibility relation. Furthermore, if the separated FEDLs in the $k_y = \pi$ plane are protected by the G_z along R-T, the separated FEDLs are in fact separated Dirac nodal chains. It should be noted that for the case of separated Dirac nodal chain, it can be divided into two parts, i.e., the FEDL in the $k_y = \pi$ plane and the accidental Dirac nodal loop in the $k_z = \pi$ plane. The evolutions of them can be deduced independently. In the following discussions, we will only focus on the evolution of FEDLs, while the evolution of the accidental Dirac nodal loop in the $k_z = \pi$ plane is neglected.

TABLE X. FEDL materials in SG.61.

Materials
AgF_2(111;2)

1. There exists only one FEDL material in SG.61 from the Materials Project. The configuration of the FEDLs contains an hourglass Dirac nodal chain traversing the BZ. More details can be obtained from the earlier work [86].

A. SG.57-sg.11 transition

The corresponding perturbation of SG.57-sg.11 transition breaks $R_{2x/y}$ and $G_{x/y}$ symmetries, while R_{2z}, G_z, and the inversion symmetries are reserved. Filling that realizes a band insulator for subgroup sg.11 is $4n$, which indicates the symmetry-enforced nodal phenomena of the subgroup are within bands from the $(4n+1)$th to the $4(n+3)$th bands. These symmetry-enforced nodal phenomena are different from the FEDLs within bands from the $(8n+3)$th to the $(8n+6)$th bands at the Fermi level. As a result, whether these systems become insulators or topological semimetals depends on how the FEDLs evolve. Furthermore, the key for the evolution of the FEDLs is to tell whether the FEDLs are protected by the preserved symmetries at the corresponding high-symmetry $\vec{k}$ points. The reason is direct, the degeneracy from the FEDL will be gapped if it is no longer protected by any reserved symmetry.

(1) R_{2z} invariant lines, R-S and T-Y: From the corresponding compatibility relations, PT related states possess the opposite R_{2z} value. Then, there exist only one irreducible representation along these two lines in sg.11, which indicates FEDLs along these lines will be gapped under SG.57-sg.11 transition.

(2) G_z invariant line, R-T: When the FEDLs are separated, they must go across R-T. From the corresponding compatibility relation, we find that PT related states along this line share the same G_z value. Then, there exist two irreducible representations with different G_z values along R-T in sg.11. Thus, band crossings from the FEDLs along R-T can be protected by G_z, which indicates that the FEDLs may be separated Dirac nodal chains. The part of accidental Dirac nodal loops (if they exist) protected by G_z in the $k_z = \pi$ plane is reserved, while the part of FEDL in the $k_y = \pi$ plane is gapped under SG.57-sg.11 transition.

In summary, the FEDLs in $k_y = \pi$ plane will be gapped, while the accidental Dirac nodal loops in $k_z = \pi$ plane (if they exist) are reserved under the SG.57-sg.11 transition. The corresponding phase transitions induced by symmetry-breaking perturbations are listed in Table III.

B. SG.57-sg.14 transition

The corresponding perturbation breaks R_{2x}, R_{2z}, G_x, and G_z symmetries, while the R_{2y}, G_y, and inversion symmetries are reserved. In this case, the FEDLs remain to be accidental Dirac nodal loops because the reserved symmetries are sufficient for Dirac nodal loops in the $k_y = \pi$ plane. How-

TABLE XI. FEDL materials in SG.205.

Materials	Materials	Materials	Materials
CuS_2(C;111,2)	Te_2Ir(C;111,3)	AuN_2(C;111,0)	IrN_2(N;111,0)
IrS_2(C;111,3)	$CuTe_2$(C;111,3)	$CoTe_2$(C;111,3)	CoS_2(C;111,2)
$CoSe_2$(C;111,2)	RhS_2(C;111,3)	$CuSe_2$(C;111,2)	Sb_2Au(C;111,3)
Te_2Rh(C;111,3)	$RhSe_2$(C;111,3)		

1. C/T/N indicates that the FEDLs consist of three separated FEDLs contractible/noncontractible in the BZ, or only one whole Dirac nodal net, respectively. The first-principles calculations indicate IrN_2 is the only material possessing the Dirac nodal net as schematized in Fig. 6(e).

ever, it should be noted that the Dirac nodal loops are no longer filling enforced. Thus, the contractible FEDLs and noncontractible FEDLs will evolve into contractible and noncontractible Dirac nodal loops, respectively.

C. SG.57-sg.28 transition

The corresponding perturbation breaks the R_{2y}, R_{2z}, G_x, and inversion symmetries, while R_{2x}, G_y, and G_z symmetries are reserved. The absence of the inversion symmetry will break the double degeneracy induced by PT, thus, each FEDL will split into two Weyl nodal loops. As a result, for the case of contractible FEDLs, each FEDL evolves into two concentric Weyl nodal loops, while for the case of noncontractible FEDLs (i.e., FEDLs traversing the BZ), each FEDL evolves into two Weyl nodal loops traversing the BZ.

D. SG.57-sg.29 transition

Similar with the SG.57-sg.28 transition, each FEDL will split into two Weyl nodal loops as a result of the breaking of the inversion symmetry. Furthermore, there exists $\Theta = G_y * T$ enforced double degeneracy along the R-T line, which indicates that for the case of separated FEDLs, the concentric Weyl nodal loops from the same FEDL touch each other along the R-T line, leading to two concentric Weyl nodal chains.

Similarly, we can deduce the evolutions of the FEDLs in the other four SGs. Especially, in terms of SG.61, class {a,b,c} of both SG.61-sg.14 and SG.61-sg.29 transitions corresponds to the axis chosen as the special direction of the symmetry-breaking perturbation, and the analyses are completely the same for the three classes due to the cyclic permutation relations shown in Table II. Furthermore, SG.205 can be seen as a cubic case of SG.61, suggesting that the three FEDLs are related to each other by the $R_{3[111]}$ symmetry. The analyses of them are very similar, as shown in Tables V and VII, respectively.

Thus, we can obtain the evolutions of the FEDLs in all the five SGs under all these transitions, the results are listed in Tables III–VII, respectively. Furthermore, some schematic figures are given to visualise these evolutions, as shown in Figs. 9 and 10, respectively.

V. POTENTIAL TIS AND TCIS FROM THE FEDL MATERIALS

In the above, we have discussed the phase transitions of the FEDL materials under symmetry-breaking but translation-invariant perturbations. One may further ask if the FEDL materials will become TIs or TCIs when the FEDLs are gapped under the corresponding perturbations. In this section, we list almost all the FEDL materials and the corresponding symmetry indicators when they become insulators under these perturbations. We import the nonmagnetic materials in the corresponding SGs that are both registered in the online crystal database the Materials Project [98] and the Inorganic Crystal Structure Database (ICSD) [99]. By "nonmagnetic," we regard one material as nonmagnetic if its magnetic moment is not higher than 0.1 μ_B per unit cell (according to its Materials Project record). Then, we select the half-filled materials (with the filling $8n + 4$) after calculating the fillings of all the materials. It is well known that each chemical element possesses "x" electrons, "x" here is just the atomic number of the chemical element. Thus, the filling of a material can be obtained by summing the atomic numbers of all the atoms in this system.

Fortunately, we find these insulators from the FEDL materials can be depicted with the $(Z_2, Z_2, Z_2; Z_4)$ indexes, just the same as centrosymmetric systems in SG.2. The values of these indexes can always be calculated for the $8n + 4$

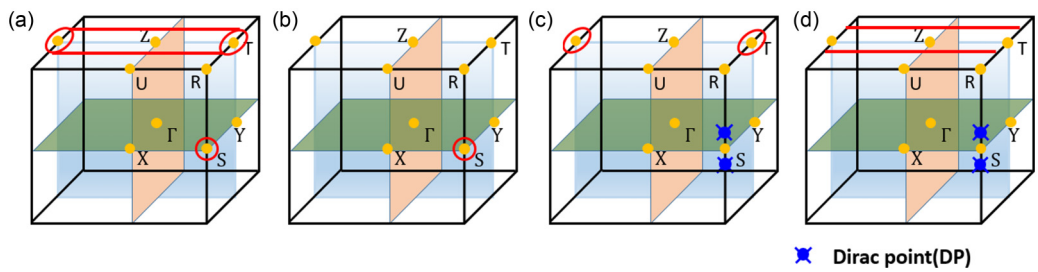

FIG. 11. (a) The schematic figure of the FEDLs for AgF_2 in SG.61. The evolution of FEDLs for AgF_2 in SG.61 under (b) SG.61-sg.14-class a, (c) SG.61-sg.14-class b, and (d) SG.61-sg.14-class c transitions, respectively. The blue discs along R-S represent Dirac points originating from the splitting of the FEDL.

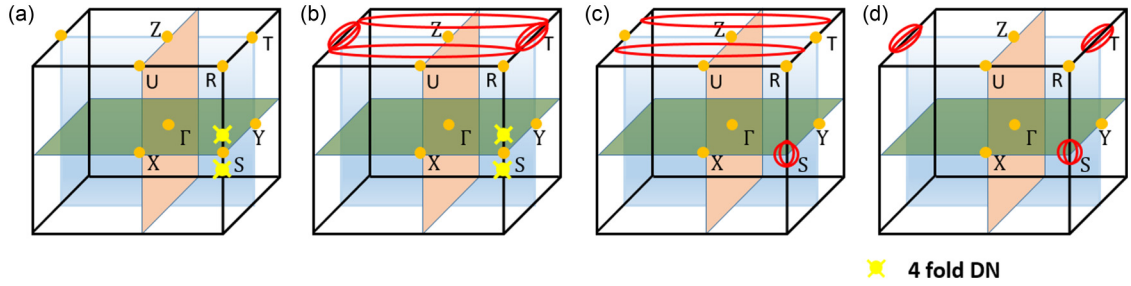

FIG. 12. The evolution of FEDLs for AgF_2 in SG.61 under (a) SG.61-sg.19, (b) SG.61-sg.29-class a, (c) SG.61-sg.29-class b, and (d) SG.61-sg.14-class c transitions, respectively. The yellow discs originating from the splitting of the FEDL in the $k_x = \pi$ plane denote the fourfold degenerate nodes (DNs) along R-S.

occupied bands and keep unchanged after these perturbations are applied. It is based on the adiabatic assumption that even though the degeneracies of the bands are violated under the perturbations, no new band crossings occur and the order of the bands keeps unchanged. The formula to calculate these indexes is expressed as

$$
\begin{aligned}
Z_{2,1} &\equiv \sum_{\substack{\mathbf{K}\in \mathbb{TRIM} \\ \text{at } \{k_x=\pi\}}} \frac{N_-(\mathbf{K}) - N_+(\mathbf{K})}{2} \bmod 2, \\
Z_{2,2} &\equiv \sum_{\substack{\mathbf{K}\in \mathbb{TRIM} \\ \text{at } \{k_y=\pi\}}} \frac{N_-(\mathbf{K}) - N_+(\mathbf{K})}{2} \bmod 2, \\
Z_{2,3} &\equiv \sum_{\substack{\mathbf{K}\in \mathbb{TRIM} \\ \text{at } \{k_z=\pi\}}} \frac{N_-(\mathbf{K}) - N_+(\mathbf{K})}{2} \bmod 2, \\
Z_4 &\equiv \sum_{\mathbf{K}\in \mathbb{TRIM}} \frac{N_-(\mathbf{K}) - N_+(\mathbf{K})}{2} \bmod 4. \qquad (10)
\end{aligned}
$$

Using the above formula, we list the corresponding $(Z_2, Z_2, Z_2; Z_4)$ indexes of almost all the FEDL materials in each SG, as shown in Tables VIII–XI, respectively.

For the case of FEDL materials in SG.62, we have listed the corresponding Z_4 index in the Supplemental Material [100], with the three other Z_2 indexes $Z_{2x} \equiv Z_{2z} \equiv 1, Z_{2y} \equiv 0$. The values of these three Z_2 indexes are always fixed, which can be seen from the following. We find only bands at U contribute to the $Z_{2x}(= Z_{2z})$ index, because bands are always fourfold degenerate with the parities $p = 2 \times (+1) \oplus 2 \times (-1)$ at the other TRIMs in the $k_x = \pi$ and $k_z = \pi$ planes. Furthermore, bands are fourfold degenerate with the parities $p = 4 \times (+1)$ or $p = 4 \times (-1)$ at U, which indicates $N_-(\mathbf{U}) - N_+(\mathbf{U}) \equiv 2 + 4m$ for the fillings of $8n + 4$, as a result, $Z_{2x} = Z_{2z} = 1$. In addition, the four TRIMs in the $k_y = \pi$ plane are all four degenerate with the parities $p = 2 \times (+1) \oplus 2 \times (-1)$, which gives $Z_{2y} = 0$.

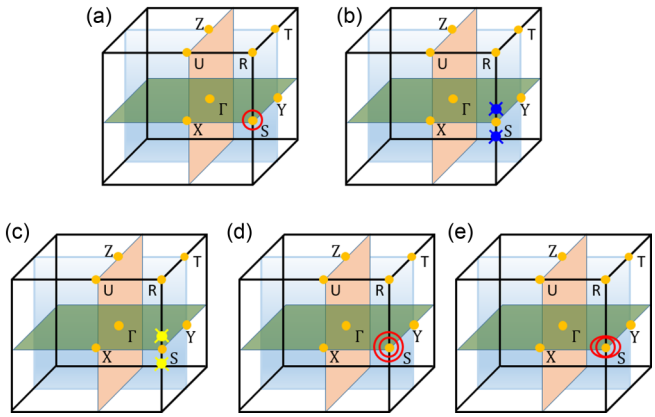

FIG. 13. The evolution of FEDLs for $SrIrO_3$ in SG.62 under (a) SG.62-sg.14-class a, (b) SG.62-sg.14-class b, (c) SG.62-sg.19, (d) SG.62-sg.31, and (e) SG.62-sg.33 transitions, respectively.

VI. TWO EXAMPLES: AgF_2 IN SG.61 AND $SrIrO_3$ IN SG.62

AgF_2 in SG.61 is an interesting FEDL material, which has been studied in the earlier work [86]. In the following, we will illustrate how this FEDL material evolves to various topological semimetals.

According to Eq. (8), we get $\{\zeta_{2x}, \zeta_{2y}, \zeta_{2z}\} = \{1, 1, 0\}$ from the first-principles calculations, which indicates the FEDLs in the $k_x = \pi \cup k_y = \pi$ and $k_z = \pi$ planes are contractible and noncontractible in the BZ, respectively. Combined with the band structures shown in Fig. 7(c), we find the contractible FEDL in the $k_x = \pi$ plane touches the noncontractible FEDL in the $k_z = \pi$ plane at some point along R-M″, leading to a Dirac nodal chain traversing the BZ, as shown in Figs. 11(a). Using Table V, and keep in mind that the node from the Dirac nodal chain along R-T is not protected by R_{2x} symmetry, while the node along R-S from the FEDL in the $k_x = \pi$ plane is protected by R_{2z} symmetry, we can easily deduce the final nodal phenomena under all the SG.61-sg.n symmetry-breaking transitions, as shown in Fig. 11 and 12, respectively.

$SrIrO_3$ in SG.62 is the well-known perovskite-class material which possesses the FEDL state [81,82]. We also deduce the evolutions of the FEDL under all maximal-subgroup transitions which respect the translation symmetries, as shown in Fig. 13.

VII. CONCLUSIONS

We propose the FEDL state in nonmagnetic systems and find it exists in five and only five SGs (SG.57, SG.60, SG.61, SG.62, and SG.205). Then we explore the possible configurations of the FEDLs in each SG. Band structures of K_2SnBi in SG.57, $Hf_2Co_3Si_4$ in SG.60, AgF_2 in SG.61, $AgAsF_7$ in SG.62, and IrN_2 in SG.205 have been calculated to show

the FEDLs in each SG. Furthermore, we study the evolutions of the FEDLs under various perturbations which respect the translation symmetries and find that the FEDL materials can serve as perfect parent materials of both topological semimetals with nodal points/loops, and TIs/TCIs. At last, almost all the FEDL materials are listed, among which we have chosen AgF_2 in SG.61 and the well-known perovskite-class material $SrIrO_3$ in SG.62 as two examples to illustrate how we can obtain various topological semimetals from the FEDL materials.

ACKNOWLEDGMENTS

We are thankful for the fruitful discussions with Huaiqiang Wang, Jiachen Gao, Zhijun Wang, Zhaopeng Guo, and Jiawei Ruan. The authors acknowledge support from Ministry of Science and Technology of China under Grant No. 2016YFA0302400, National Science Foundation of China under Grant No. 11674370, and Chinese Academy of Sciences under Grants No. XXH13506-202 and No. XDB33000000.

[1] M. Z. Hasan and C. L. Kane, Rev. Mod. Phys. **82**, 3045 (2010).
[2] X.-L. Qi and S.-C. Zhang, Rev. Mod. Phys. **83**, 1057 (2011).
[3] N. P. Armitage, E. J. Mele, and A. Vishwanath, Rev. Mod. Phys. **90**, 015001 (2018).
[4] C. L. Kane and E. J. Mele, Phys. Rev. Lett. **95**, 226801 (2005).
[5] X. Wan, A. M. Turner, A. Vishwanath, and S. Y. Savrasov, Phys. Rev. B **83**, 205101 (2011).
[6] G. Xu, H. Weng, Z. Wang, X. Dai, and Z. Fang, Phys. Rev. Lett. **107**, 186806 (2011).
[7] K.-Y. Yang, Y.-M. Lu, and Y. Ran, Phys. Rev. B **84**, 075129 (2011).
[8] A. A. Burkov and L. Balents, Phys. Rev. Lett. **107**, 127205 (2011).
[9] A. A. Burkov, M. D. Hook, and L. Balents, Phys. Rev. B **84**, 235126 (2011).
[10] G. B. Halász and L. Balents, Phys. Rev. B **85**, 035103 (2012).
[11] A. A. Zyuzin, S. Wu, and A. A. Burkov, Phys. Rev. B **85**, 165110 (2012).
[12] L. Lu, L. Fu, J. Joannopoulos, and M. Soljacic, Nat. Photonics **7**, 294 (2012).
[13] T. Das, Phys. Rev. B **88**, 035444 (2013).
[14] J. Liu and D. Vanderbilt, Phys. Rev. B **90**, 155316 (2014).
[15] H. Zhang, J. Wang, G. Xu, Y. Xu, and S.-C. Zhang, Phys. Rev. Lett. **112**, 096804 (2014).
[16] H. Weng, C. Fang, Z. Fang, B. A. Bernevig, and X. Dai, Phys. Rev. X **5**, 011029 (2015).
[17] S.-Y. Xu, I. Belopolski, N. Alidoust, M. Neupane, G. Bian, C. Zhang, R. Sankar, G. Chang, Z. Yuan, C.-C. Lee, S.-M. Huang, H. Zheng, J. Ma, D. S. Sanchez, B. Wang, A. Bansil, F. Chou, P. P. Shibayev, H. Lin, S. Jia, and M. Z. Hasan, Science **349**, 613 (2015).
[18] B. Q. Lv, H. M. Weng, B. B. Fu, X. P. Wang, H. Miao, J. Ma, P. Richard, X. C. Huang, L. X. Zhao, G. F. Chen, Z. Fang, X. Dai, T. Qian, and H. Ding, Phys. Rev. X **5**, 031013 (2015).
[19] L. X. Yang, Z. K. Liu, Y. Sun, H. Peng, H. F. Yang, T. Zhang, B. Zhou, Y. Zhang, Y. F. Guo, M. Rahn, D. Prabhakaran, Z. Hussain, S.-K. Mo, C. Felser, B. Yan, and Y. L. Chen, Nat. Phys. **11**, 879 (2015).
[20] B. Q. Lv, B. Q. Lv, N. Xu, H. M. Weng, J. Z. Ma, P. Richard, X. C. Huang, L. X. Zhao, G. F. Chen, C. E. Matt, F. Bisti, V. N. Strocov, J. Mesot, Z. Fang, X. Dai, T. Qian, M. Shi, and H. Ding, Nat. Phys. **11**, 724 (2015).
[21] S.-Y. Xu, I. Belopolski, D. S. Sanchez, C. Zhang, G. Chang, C. Guo, G. Bian, Z. Yuan, H. Lu, T.-R. Chang, P. P. Shibayev, M. L. Prokopovych, N. Alidoust, H. Zheng, C.-C. Lee, S.-M. Huang, R. Sankar, F. Chou, C.-H. Hsu, H.-T. Jeng, A. Bansil, T. Neupert, V. N. Strocov, H. Lin, S. Jia, and M. Z. Hasan, Sci. Adv. **1**, e1501092 (2015).
[22] N. Alidoust, S. Y. Xu, I. Belopolski, G. Bian, H. Zheng, D. S. Sanchez, T. Neupert, M. Z. Hasan, Z. Yuan, and C. Zhang, Nat. Phys. **11**, 748 (2015).
[23] S.-M. Huang, S.-Y. Xu, I. Belopolski, C.-C. Lee, G. Chang, B. Wang, N. Alidoust, G. Bian, M. Neupane, C. Zhang, S. Jia, A. Bansil, H. Lin, and M. Z. Hasan, Nat. Commun. **6**, 7373 (2015).
[24] N. Xu, H. M. Weng, B. Q. Lv, C. E. Matt, J. Park, F. Bisti, V. N. Strocov, D. Gawryluk, E. Pomjakushina, and K. Conder, Nat. Commun. **7**, 11006 (2016).
[25] L. Lu, Z. Wang, D. Ye, L. Ran, L. Fu, J. D. Joannopoulos, and M. Soljačić, Science **349**, 622 (2015).
[26] J. Ruan, S. K. Jian, H. Yao, H. Zhang, S. C. Zhang, and D. Xing, Nat. Commun. **7**, 11136 (2016).
[27] J. Ruan, S.-K. Jian, D. Zhang, H. Yao, H. Zhang, S.-C. Zhang, and D. Xing, Phys. Rev. Lett. **116**, 226801 (2016).
[28] A. P. Schnyder, S. Ryu, A. Furusaki, and A. W. W. Ludwig, Phys. Rev. B **78**, 195125 (2008).
[29] A. Kitaev, in *Advances in Theoretical Physics: Landau Memorial Conference*, edited by V. Lebedev and M. Feigel'man, AIP Conf. Proc. No. 1134 (AIP, New York, 2009).
[30] L. Fu, Phys. Rev. Lett. **106**, 106802 (2011).
[31] R.-J. Slager, A. Mesaros, V. Juricic, and J. Zaanen, Nat. Phys. **9**, 98 (2013).
[32] P. Jadaun, D. Xiao, Q. Niu, and S. K. Banerjee, Phys. Rev. B **88**, 085110 (2013).
[33] K. Shiozaki and M. Sato, Phys. Rev. B **90**, 165114 (2014).
[34] Z. Wang, A. Alexandradinata, R. J. Cava, and B. A. Bernevig, Nature (London) **532**, 189 (2016).
[35] Z. Song, T. Zhang, Z. Fang, and C. Fang, Nat. Commun. **9**, 3530 (2018).
[36] E. Khalaf, H. C. Po, A. Vishwanath, and H. Watanabe, Phys. Rev. X **8**, 031070 (2018).
[37] Z. Song, S.-J. Huang, Y. Qi, C. Fang, and M. Hermele, Sci. Adv. **5**, eaax2007 (2019).
[38] B. Bradlyn, L. Elcoro, J. Cano, M. G. Vergniory, Z. Wang, C. Felser, M. I. Aroyo, and B. A. Bernevig, Nature (London) **547**, 298 (2017).
[39] H. C. Po, A. Vishwanath, and H. Watanabe, Nat. Commun. **8**, 50 (2017).
[40] J. Kruthoff, J. de Boer, J. van Wezel, C. L. Kane, and R.-J. Slager, Phys. Rev. X **7**, 041069 (2017).
[41] M. G. Vergniory, L. Elcoro, C. Felser, N. Regnault, B. A. Bernevig, and Z. Wang, Nature (London) **566**, 480 (2019).
[42] T. Zhang, Y. Jiang, Z. Song, H. Huang, Y. He, Z. Fang, H. Weng, and C. Fang, Nature (London) **566**, 475 (2019).
[43] F. Tang, H. C. Po, A. Vishwanath, and X. Wan, Nature (London) **566**, 486 (2019).

[44] J. Cano, B. Bradlyn, Z. Wang, L. Elcoro, M. G. Vergniory, C. Felser, M. I. Aroyo, and B. A. Bernevig, Phys. Rev. Lett. **120**, 266401 (2018).

[45] B. Bradlyn, L. Elcoro, M. G. Vergniory, J. Cano, Z. Wang, C. Felser, M. I. Aroyo, and B. A. Bernevig, Phys. Rev. B **97**, 035138 (2018).

[46] J. Cano, B. Bradlyn, Z. Wang, L. Elcoro, M. G. Vergniory, C. Felser, M. I. Aroyo, and B. A. Bernevig, Phys. Rev. B **97**, 035139 (2018).

[47] Z. Wang, Y. Sun, X.-Q. Chen, C. Franchini, G. Xu, H. Weng, X. Dai, and Z. Fang, Phys. Rev. B **85**, 195320 (2012).

[48] S. M. Young, S. Zaheer, J. C. Y. Teo, C. L. Kane, E. J. Mele, and A. M. Rappe, Phys. Rev. Lett. **108**, 140405 (2012).

[49] Z. Wang, H. Weng, Q. Wu, X. Dai, and Z. Fang, Phys. Rev. B **88**, 125427 (2013).

[50] Z. K. Liu, J. Jiang, B. Zhou, Z. J. Wang, Y. Zhang, H. M. Weng, D. Prabhakaran, S. K. Mo, H. Peng, and P. Dudin, Nat. Mater. **13**, 677 (2014).

[51] Y. L. Chen, Z. K. Liu, B. Zhou, Y. Zhang, Z. J. Wang, H. M. Weng, D. Prabhakran, S. K. Mo, Z. X. Shen, and Z. Fang, Science **343**, 864 (2014).

[52] M. Neupane, S. Y. Xu, R. Sankar, N. Alidoust, G. Bian, C. Liu, I. Belopolski, T. R. Chang, H. T. Jeng, and H. Lin, Nat. Commun. **5**, 3786 (2014).

[53] B.-J. Yang and N. Nagaosa, Nat. Commun. **5**, 4898 (2014).

[54] S. Y. Xu, C. Liu, S. K. Kushwaha, R. Sankar, J. W. Krizan, I. Belopolski, M. Neupane, G. Bian, N. Alidoust, and T. R. Chang, Science **347**, 294 (2015).

[55] C.-Z. Xu, Y.-H. Chan, Y. Chen, P. Chen, X. Wang, C. Dejoie, M.-H. Wong, J. A. Hlevyack, H. Ryu, H.-Y. Kee, N. Tamura, M.-Y. Chou, Z. Hussain, S.-K. Mo, and T.-C. Chiang, Phys. Rev. Lett. **118**, 146402 (2017).

[56] H. Huang and F. Liu, Phys. Rev. B **95**, 201101(R) (2017).

[57] P. Tang, Q. Zhou, G. Xu, and S.-C. Zhang, Nat. Phys. **12**, 1100 (2016).

[58] J. Wang, Phys. Rev. B **95**, 115138 (2017).

[59] D. Zhang, H. Wang, J. Ruan, G. Yao, and H. Zhang, Phys. Rev. B **97**, 195139 (2018).

[60] G. Hua, S. Nie, Z. Song, R. Yu, G. Xu, and K. Yao, Phys. Rev. B **98**, 201116(R) (2018).

[61] J. Zhang, Y.-H. Chan, C.-K. Chiu, M. G. Vergniory, L. M. Schoop, and A. P. Schnyder, Phys. Rev. Mater. **2**, 074201 (2018).

[62] Y. Kim, B. J. Wieder, C. L. Kane, and A. M. Rappe, Phys. Rev. Lett. **115**, 036806 (2015).

[63] R. Yu, H. Weng, Z. Fang, X. Dai, and X. Hu, Phys. Rev. Lett. **115**, 036807 (2015).

[64] G. Bian, T.-R. Chang, H. Zheng, S. Velury, S.-Y. Xu, T. Neupert, C.-K. Chiu, S.-M. Huang, D. S. Sanchez, I. Belopolski, N. Alidoust, P.-J. Chen, G. Chang, A. Bansil, H.-T. Jeng, H. Lin, and M. Z. Hasan, Phys. Rev. B **93**, 121113(R) (2016).

[65] C. Fang, H. Weng, X. Dai, and Z. Fang, Chin. Phys. B **25**, 117106 (2016).

[66] R. Yu, Z. Fang, X. Dai, and H. Weng, Front. Phys. **12**, 127202 (2017).

[67] S. Li, Z.-M. Yu, Y. Liu, S. Guan, S.-S. Wang, X. Zhang, Y. Yao, and S. A. Yang, Phys. Rev. B **96**, 081106(R) (2017).

[68] Y. Sun, Y. Zhang, C.-X. Liu, C. Felser, and B. Yan, Phys. Rev. B **95**, 235104 (2017).

[69] G. Chang, S.-Y. Xu, X. Zhou, S.-M. Huang, B. Singh, B. Wang, I. Belopolski, J. Yin, S. Zhang, A. Bansil, H. Lin, and M. Z. Hasan, Phys. Rev. Lett. **119**, 156401 (2017).

[70] Q.-F. Liang, J. Zhou, R. Yu, Z. Wang, and H. Weng, Phys. Rev. B **93**, 085427 (2016).

[71] C. Zhong, Y. Chen, Y. Xie, S. A. Yang, M. L. Cohen, and S. B. Zhang, Nanoscale **8**, 7232 (2016).

[72] T. Bzdušek and M. Sigrist, Phys. Rev. B **96**, 155105 (2017).

[73] S. Guan, Y. Liu, Z.-M. Yu, S.-S. Wang, Y. Yao, and S. A. Yang, Phys. Rev. Mater. **1**, 054003 (2017).

[74] W. Wu, Y. Liu, S. Li, C. Zhong, Z.-M. Yu, X.-L. Sheng, Y. X. Zhao, and S. A. Yang, Phys. Rev. B **97**, 115125 (2018).

[75] W. Chen, H.-Z. Lu, and J.-M. Hou, Phys. Rev. B **96**, 041102(R) (2017).

[76] Z. Yan, R. Bi, H. Shen, L. Lu, S.-C. Zhang, and Z. Wang, Phys. Rev. B **96**, 041103(R) (2017).

[77] B. Bradlyn, J. Cano, Z. Wang, M. G. Vergniory, C. Felser, R. J. Cava, and B. A. Bernevig, Science **353**, aaf5037 (2016).

[78] B. J. Wieder, Y. Kim, A. M. Rappe, and C. L. Kane, Phys. Rev. Lett. **116**, 186402 (2016).

[79] Z. Song, T. Zhang, and C. Fang, Phys. Rev. X **8**, 031069 (2018).

[80] H. Watanabe, H. C. Po, M. P. Zaletel, and A. Vishwanath, Phys. Rev. Lett. **117**, 096404 (2016).

[81] M. A. Zeb and H.-Y. Kee, Phys. Rev. B **86**, 085149 (2012).

[82] Y. Chen, Y.-M. Lu, and H.-Y. Kee, Nat. Commun. **6**, 6593 (2015).

[83] S.-S. Wang, Y. Liu, Z.-M. Yu, X.-L. Sheng, and S. A. Yang, Nat. Commun. **8**, 1844 (2017).

[84] S. Li, Y. Liu, S.-S. Wang, Z.-M. Yu, S. Guan, X.-L. Sheng, Y. Yao, and S. A. Yang, Phys. Rev. B **97**, 045131 (2018).

[85] T.-S. Nam, C.-J. Kang, D.-C. Ryu, J. Kim, H. Kim, K. Kim, and B. I. Min, Phys. Rev. B **99**, 125115 (2019).

[86] D. Shao, H. Wang, T. Chen, P. Lu, Q. Gu, L. Sheng, D. Xing, and J. Sun, npj Comput. Mater. **5**, 53 (2019).

[87] R. Yu, W. Zhang, H.-J. Zhang, S.-C. Zhang, X. Dai, and Z. Fang, Science **329**, 61 (2010).

[88] N. Levy, S. A. Burke, K. L. Meaker, M. Panlasigui, A. Zettl, F. Guinea, A. H. Castro Neto, and M. F. Crommie, Science **329**, 544 (2010).

[89] C. Chang, J. Zhang, X. Feng, J. Shen, Z. Zhang, M. Guo, K. Li, Y. Ou, P. Wei, and L. Wang, Science **340**, 167 (2013).

[90] D. Shao, J. Ruan, J. Wu, T. Chen, Z. Guo, H. Zhang, J. Sun, L. Sheng, and D. Xing, Phys. Rev. B **96**, 075112 (2017).

[91] G. Kresse and D. Joubert, Phys. Rev. B **59**, 1758 (1999).

[92] J. P. Perdew, K. Burke, and M. Ernzerhof, Phys. Rev. Lett. **77**, 3865 (1996).

[93] H. J. Monkhorst and J. D. Pack, Phys. Rev. B **13**, 5188 (1976).

[94] T. Bzdusek, Q. Wu, A. Ruegg, M. Sigrist, and A. A. Soluyanov, Nature (London) **538**, 75 (2016).

[95] C. Fang, Y. Chen, H.-Y. Kee, and L. Fu, Phys. Rev. B **92**, 081201(R) (2015).

[96] M. I. Aroyo, A. Kirov, C. Capillas, J. M. Perez-Mato, and H. Wondratschek, Acta Crystallogr. Sect. A **62**, 115 (2006).

[97] M. I. Aroyo, J. M. Perez-Mato, D. Orobengoa, E. Tasci, G. de la Flor, and A. Kirov, Bulg. Chem. Commun. **43**, 183 (2011).

[98] A. Jain, S. P. Ong, G. Hautier, and C. Wei, APL Mater. **1**, 011002 (2013); https://materialsproject.org.

[99] M. Hellenbrandt, Crystallogr. Rev. **10**, 17 (2004); https://icsd.fiz-karlsruhe.de/index.xhtml.

[100] See Supplemental Material at http://link.aps.org/supplemental/10.1103/PhysRevB.102.165135 for the corresponding Z_4 index of the FEDL materials in SG.62.